Electronic Supplementary Material (ESI) for Nanoscale.

Supporting Information

Phase-selective synthesis of self-supported RuP film for efficient hydrogen evolution electrocatalysis in alkaline media

Ruixiang Ge, Shuo Wang, Jianwei Su, Yan Dong, Yichao Lin, Qiuju Zhang, and Liang Chen**

Experimental Section

Materials: Ruthenium chloride hydrate ($RuCl_3 \cdot xH_2O$), sodium hypophosphite (NaH_2PO_2), polyvinylpyrrolidone (PVP, K-30), N,N-Dimethylformamide (DMF), and copper sulfate pentahydrate ($CuSO_4 \cdot 5H_2O$) were purchased from Aladdin Ltd. (Shanghai, China). Pt/C (20 wt%) was purchased from Alfa Aesar Chemical Reagent Co., Ltd. The CC substrate is commercially available, and was treated with nitric acid (68 %wt) at 120 ℃ for 2 h to enhance the hydrophilicity. Deionized water was used throughout all experiments. All reagents were used as received.

Preparation of RuP/CC and RuP_2/CC: 1.56 g $RuCl_3 \cdot xH_2O$ and 0.25 g PVP were dissolved into DMF under magnetic stirring. The resulting solution was diluted to 10 mL with DMF and was stored under dark condiction for further use. A piece of CC (1 cm × 2 cm) was dipped into the above solution for 5 s. After drying under 80 ℃, the obtained carbon cloth and 1.0 g NaH_2PO_2 were heated at 600 ℃for 2h (ramping rate: 5 ℃/min) in a static Ar atmosphere. A $CuSO_4$ solution was used to absorb the released gas. Illustration of the experimental setup is shown in Fig. S18. RuP_2/CC was prepared by identical method, except that 4.0 g NaH_2PO_2 was used. The loading mass of RuP and RuP_2 was determined using a high precision microbalance. The mass of Ru and P were determined by inductively coupled plasma optical emission spectrometer (ICP-OES). The results are listed in Tab. S3.

Characterizations: The XRD analysis of all samples were carried out on a Rigaku D/MAX-γA diffractometer with Cu Kα radiation (λ = 1.54178 Å). The SEM and TEM images were taken from a Hitachi S-4800 field emission scanning electron microscope and a Talos F200X microscope, respectively. The XPS scans were performed on a Shimadzu/Kratos AXIS Ultra XPS spectrometer. All XPS spectra were corrected using the C 1s peak at 284.8 eV. ICP-OES results were obtained from a PE 2100 DV analyzer.

Electrochemical measurements: The electrochemical performances of all samples were tested using a CHI 760E electrochemical analyzer (CH Instruments, Inc., Shanghai) in a three-electrode cell. An Ag/AgCl electrode was used as the reference electrode, and a graphite rod serves as the counter electrode. All the electrochemical measurements were performed in 1.0 M KOH. The current densities were calculated with respect to the geometrical area of the electrodes (0.5 cm × 0.5 cm). The potential was reported on reversible hydrogen electrode (RHE) scale unless specific statement. A scan rate of 0.5 mV s^{-1} was adopted to collect the polarization curves. The EIS measurements were performed with a 5 mV amplitude and a frequency range from 100,000 to 0.01 Hz. All experiments were carried out at 25 °C.

Faradic efficiency calculation：To measure the Faradic efficiency, an H-type cell was used as the reaction system and was purged with Ar for 60 min to remove air. The Ar gas flow rate for cathodic chamber was set as 10 mL min^{-1}. The gas flow was introduced directly to the gas sample loop of gas chromatograph (Agilent 7890B) for gas analysis. The practical hydrogen generation rate was calculated using the following equation: practical hydrogen generation rate = $c\ v\ t$ / (24.8 L mol^{-1}), where c is the concentration (ppm) of H_2, v is the outlet gas flow rate (10 mL min^{-1}), t is time (1 min) and 24.8 is the volume of 1 mol H_2 at 25 °C. Chronopotentiometric electrolysis was performed for 1 h before each test. Theoretical hydrogen generation rate was calculated by the following equation: theoretical hydrogen generation rate = $j\ A\ t\ /\ 2\ F$, where j is the current density, A is the geometric area of the electrode; 2 indicates the mole of electrons consumed for evolving one mole of H_2 from water; F is the Faradic constant (96,485 C mol^{-1}). The Faradic efficiency is obtained by comparing the practical hydrogen generation rate with the theoretical one.

Computational details: Spin-polarized density functional theory calculations were performed using the Vienna ab initio simulation package (VASP).[1-3] We used the RPBE functional for the exchange-correlation energy[4] and projector augmented wave (PAW) potentials.[5,6] The kinetic energy cutoff was set to 450 eV. The ionic relaxation was performed until the force on each atom is less than 0.02 eV/Å. The k-points meshes were 7×7×1 with Monkhorst-Pack method.[7] The simulations were performed based on a RuP (101) and RuP_2 (121) slab model. To minimize the undesired interactions between images, a vacuum of at least 10 Å was considered along the z axis. HSE06 calculation is performed to obtain the total density of states for these two surfaces.[8]

The free energy change for H* adsorption on catalyst surfaces (ΔG_H) was calculated as follows, which is proposed by Norskov and coworkers:[9]

$$\Delta G_H = E_{total} - E_{sur} - E_H{}^2/2 + \Delta E_{ZPE} - T\Delta S \qquad (1)$$

where E_{total} is the total energy for the adsorption state, E_{sur} is the energy of pure surface, $E_H{}^2$ is the energy of H_2 in gas phase, ΔE_{ZPE} is the zero-point energy change and ΔS is the entropy change.

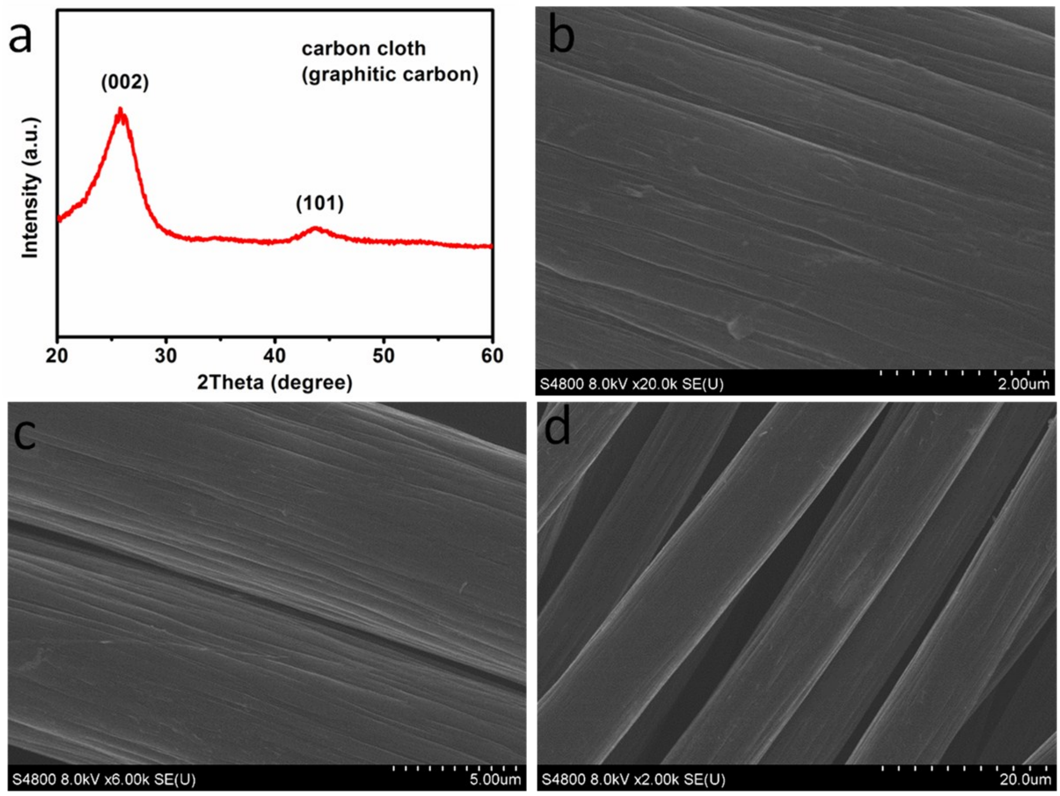

Fig. S1. (a) XRD pattern of CC (b-d) SEM images of bare CC.

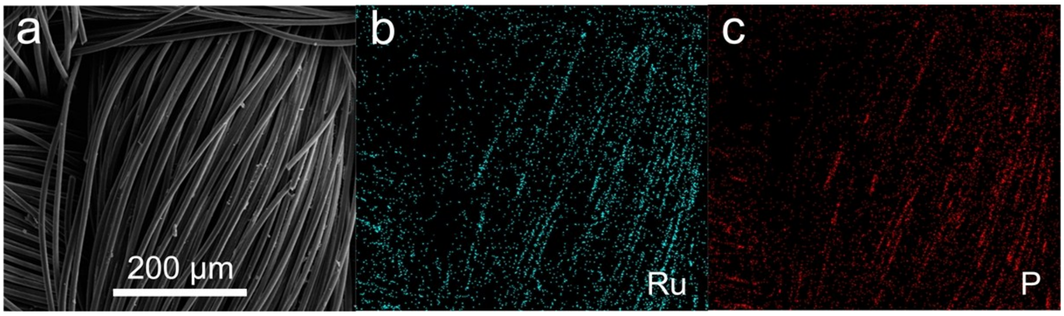

Fig. S2. (a) SEM image of RuP/CC and corresponding EDX mapping images for (b) Ru and (c) P.

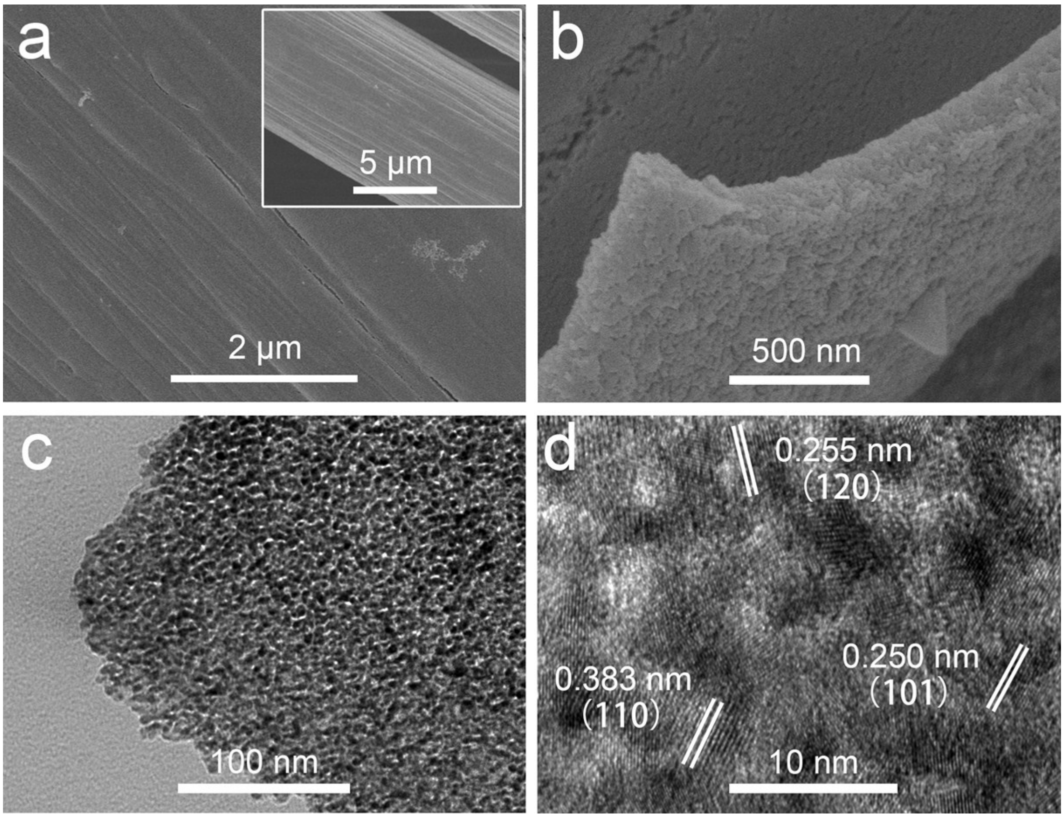

Fig. S3. (a) Top view SEM image of RuP_2/CC. Inset is low-magnification image. (b) Cross-sectional SEM image of RuP_2 film. (c) (d) HRTEM images of RuP_2 film.

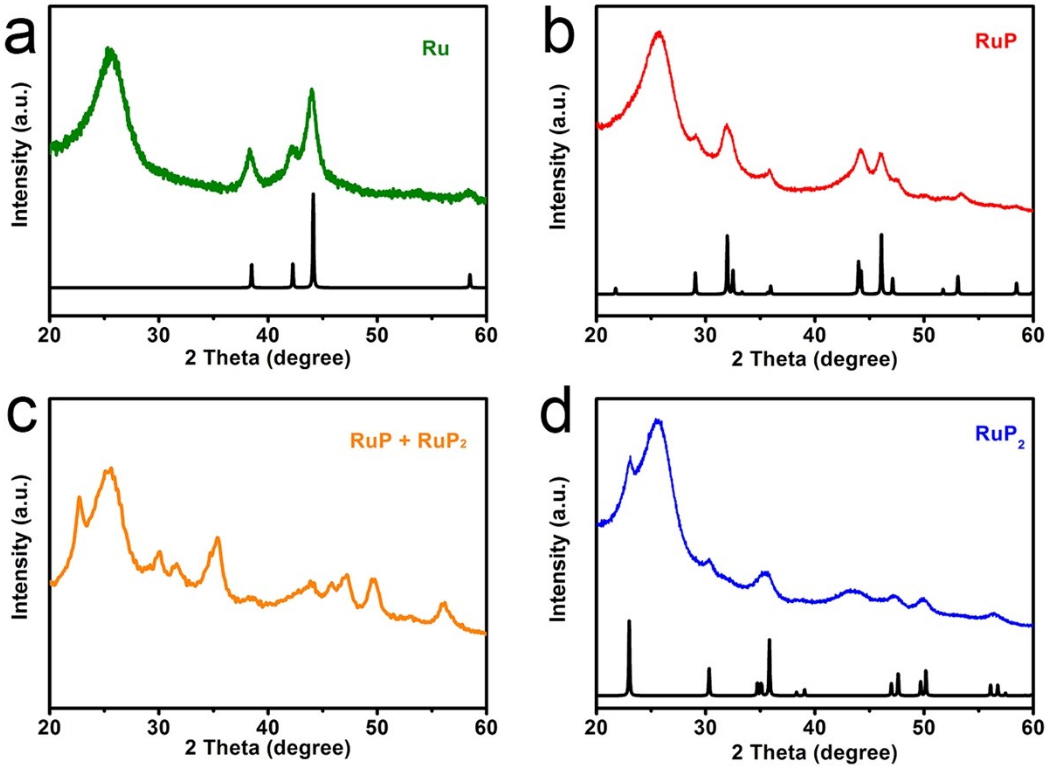

Fig. S4. XRD patterns of the samples prepared using (a) 0.5 g, (b) 1.0 g, (c) 2.0 g, and (d) 4.0 g of NaH_2PO_2

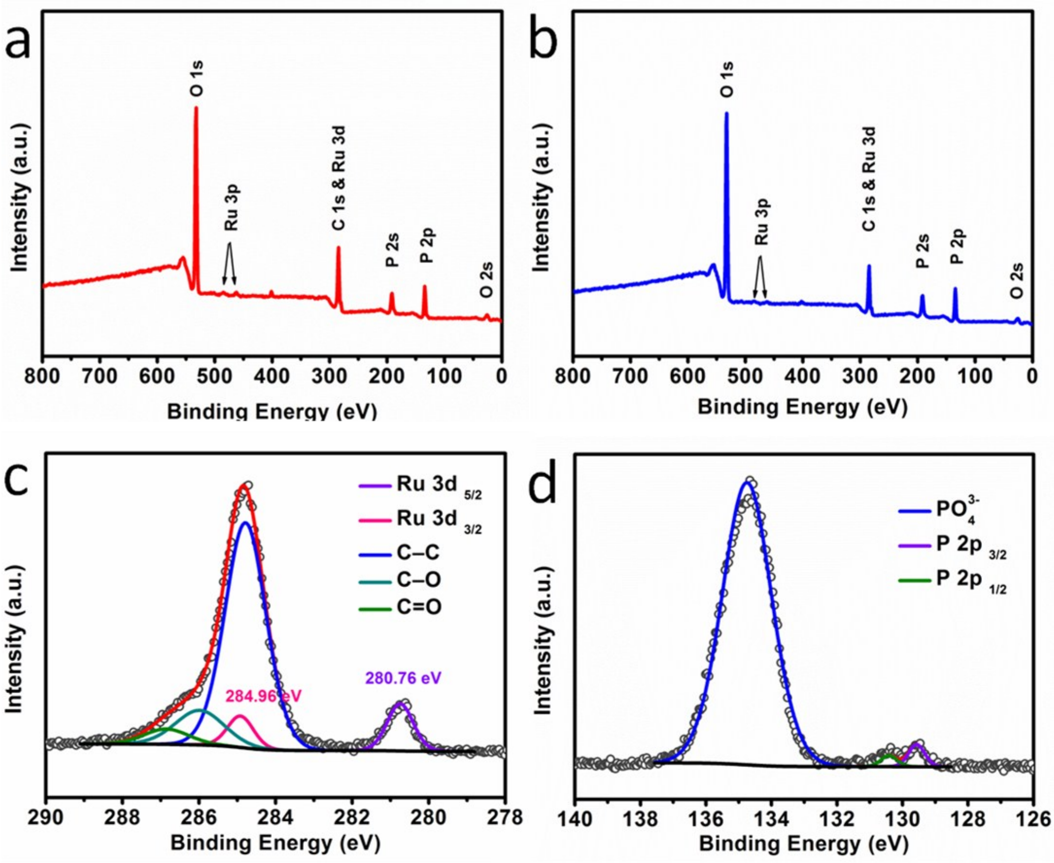

Fig. S5. XPS survey spectra of (a) RuP/CC and (b) RuP_2/CC. XPS spectra of RuP_2/CC in the (c) Ru 3d and C 1s, and (d) P 2p regions.

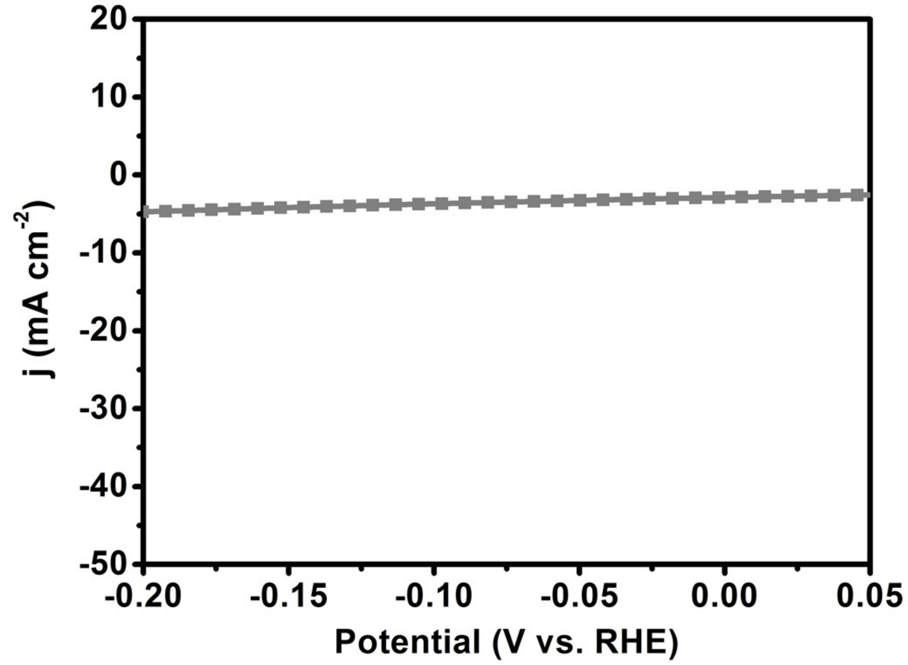

Fig. S6. LSV curve of CC after phosphorization treatment.

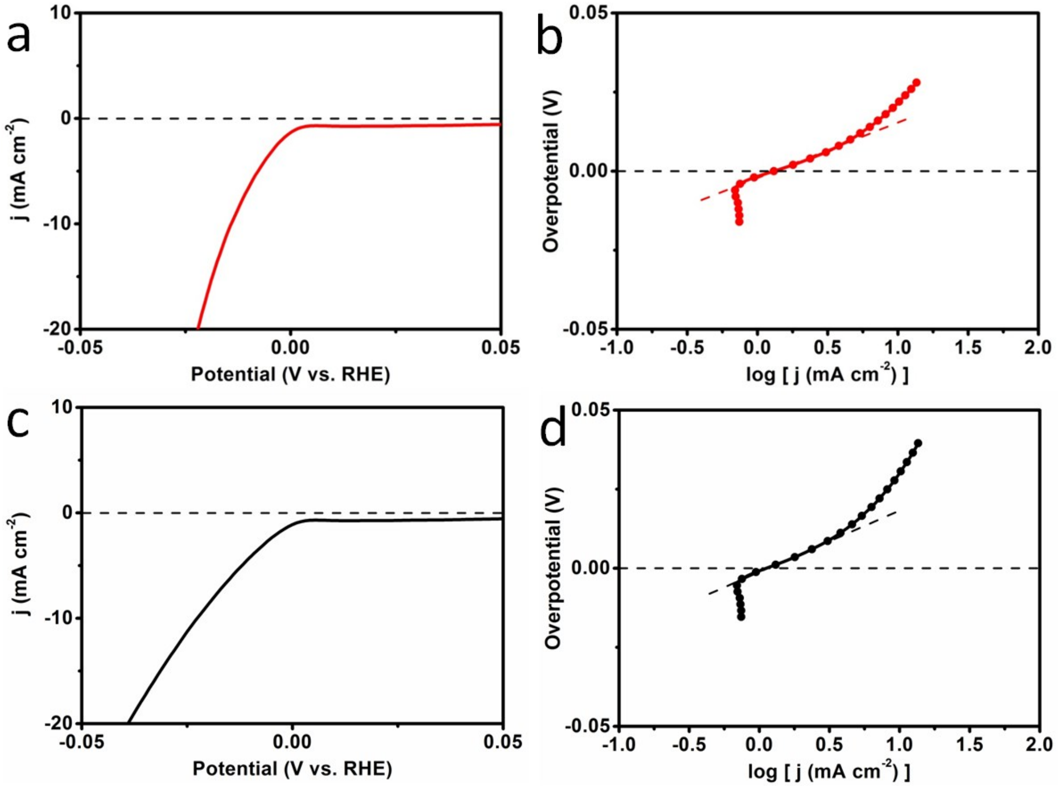

Fig. S7. (a) The iR-corrected LSV curve of RuP/CC. (b) The Tafel plot derived from iR-corrected LSV curve of RuP/CC. (c) The LSV curve of RuP/CC without iR-correction. (d) The Tafel plot derived from the LSV curve of RuP/CC without iR-correction.

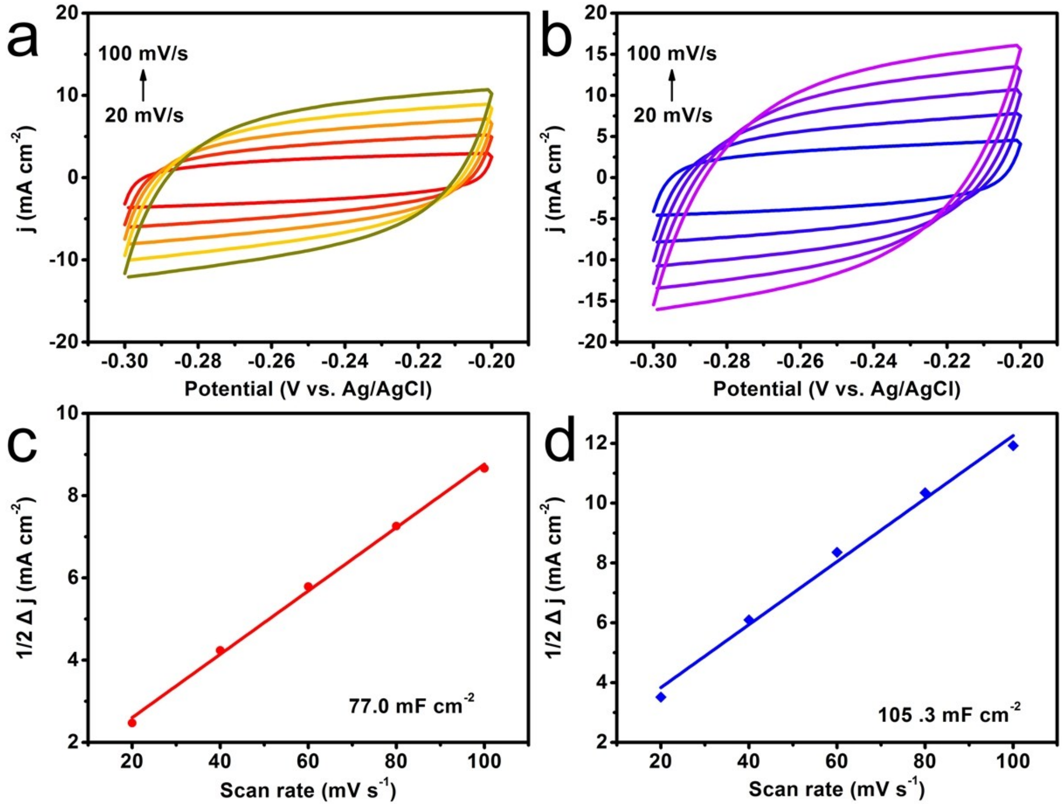

Fig. S8. CV curves at various scan rates (20, 40, 60, 80, and 100 mV s^{-1}) for (a) RuP/CC and (b) RuP$_2$/CC in 1.0 M KOH. Plots showing the extraction of the double-layer capacitances for (c) RuP/CC and (d) RuP$_2$/CC.

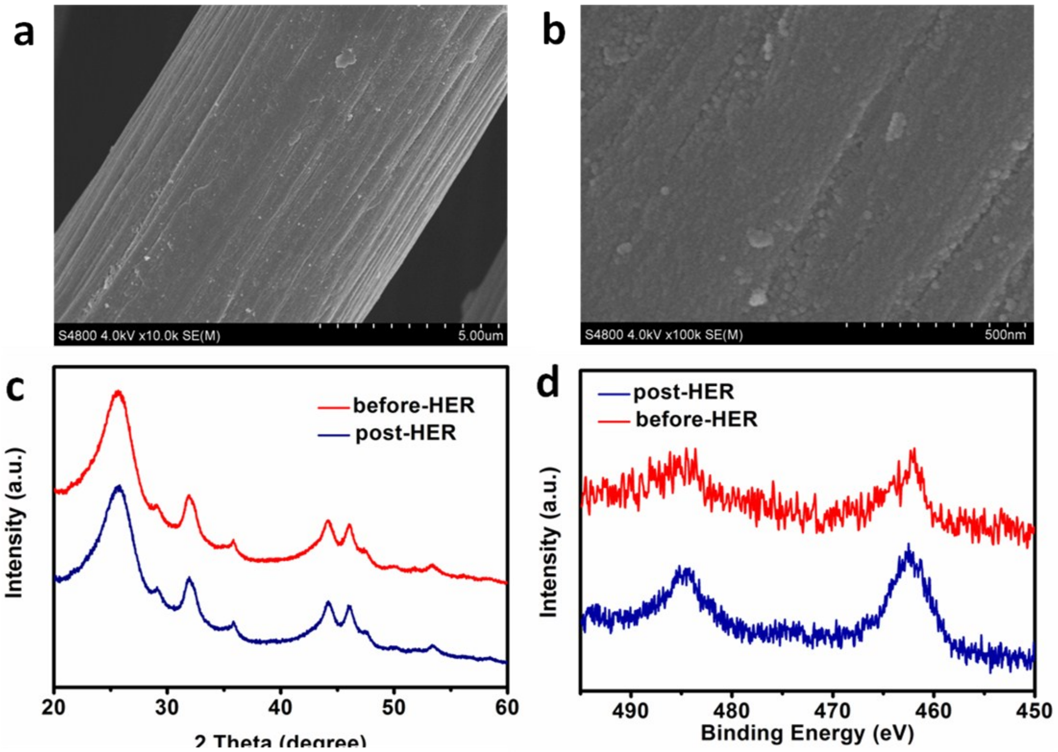

Fig. S9. (a), (b) SEM images of RuP/CC after stability test. (c) XRD pattern of RuP/CC after stability test. (d) Ru 3p spetra of RuP/CC after stability test.

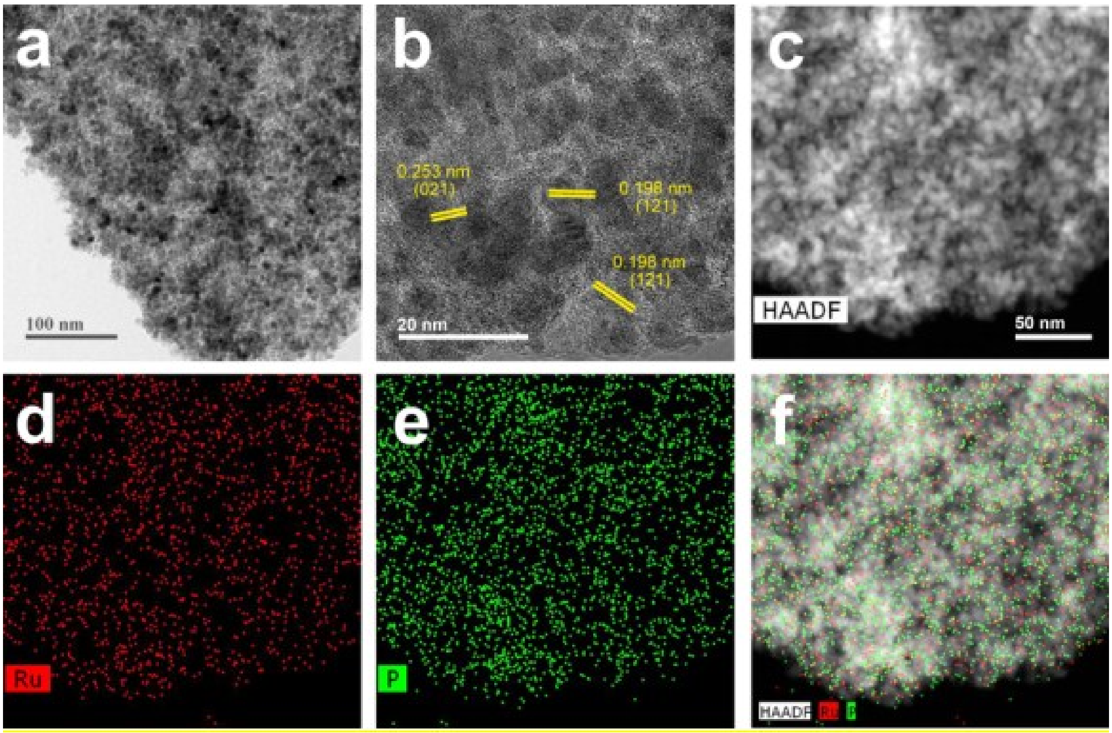

Fig. S10. (a) TEM and (b) HRTEM images of RuP after stability test. (c) HAADF-STEM image and (d) (e) (f) the corresponding EDX mapping images for Ru and P.

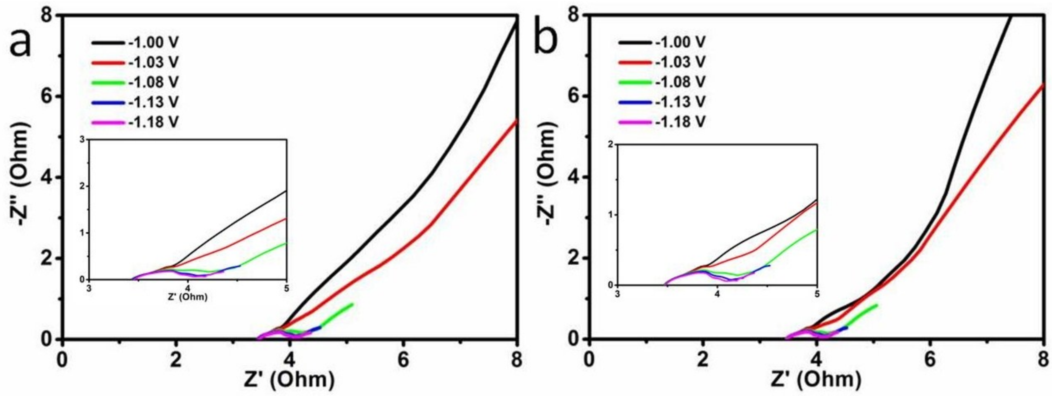

Fig. S11. (a) Nyquist plots of the same RuP/CC sample under different potentials (vs. Ag/AgCl) before stability test and (b) after stability test. The corresponding R_{ct} values are listed in Table S1. The EIS measurements were performed with a 5 mV amplitude and a frequency range from 100,000 to 0.1 Hz. Insets shows the enlarged spectra.

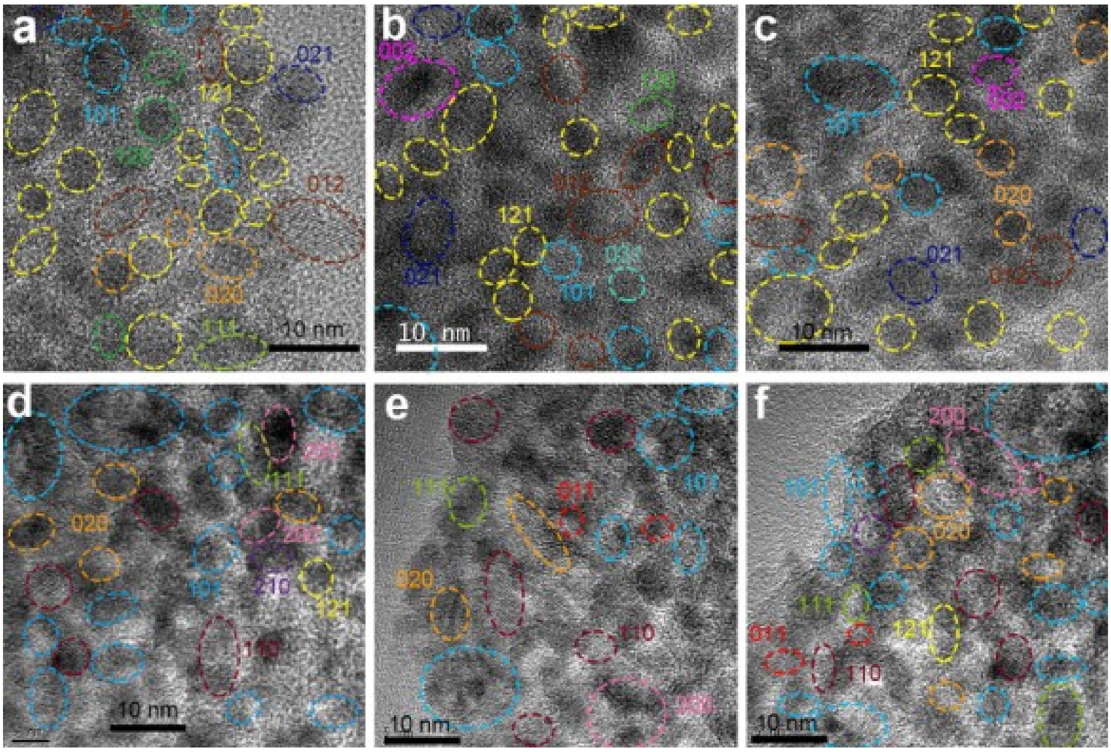

Fig. S12. (a)(b)(c) HRTEM images taken from different regions of RuP; (d)(e)(f) HRTEM images taken from different regions of RuP_2. All the present planes were identified by measuring the interlayer distances of well-resolved lattice fringes, and typical integral intensity profiles are shown in Figure S11 and Figure S12.

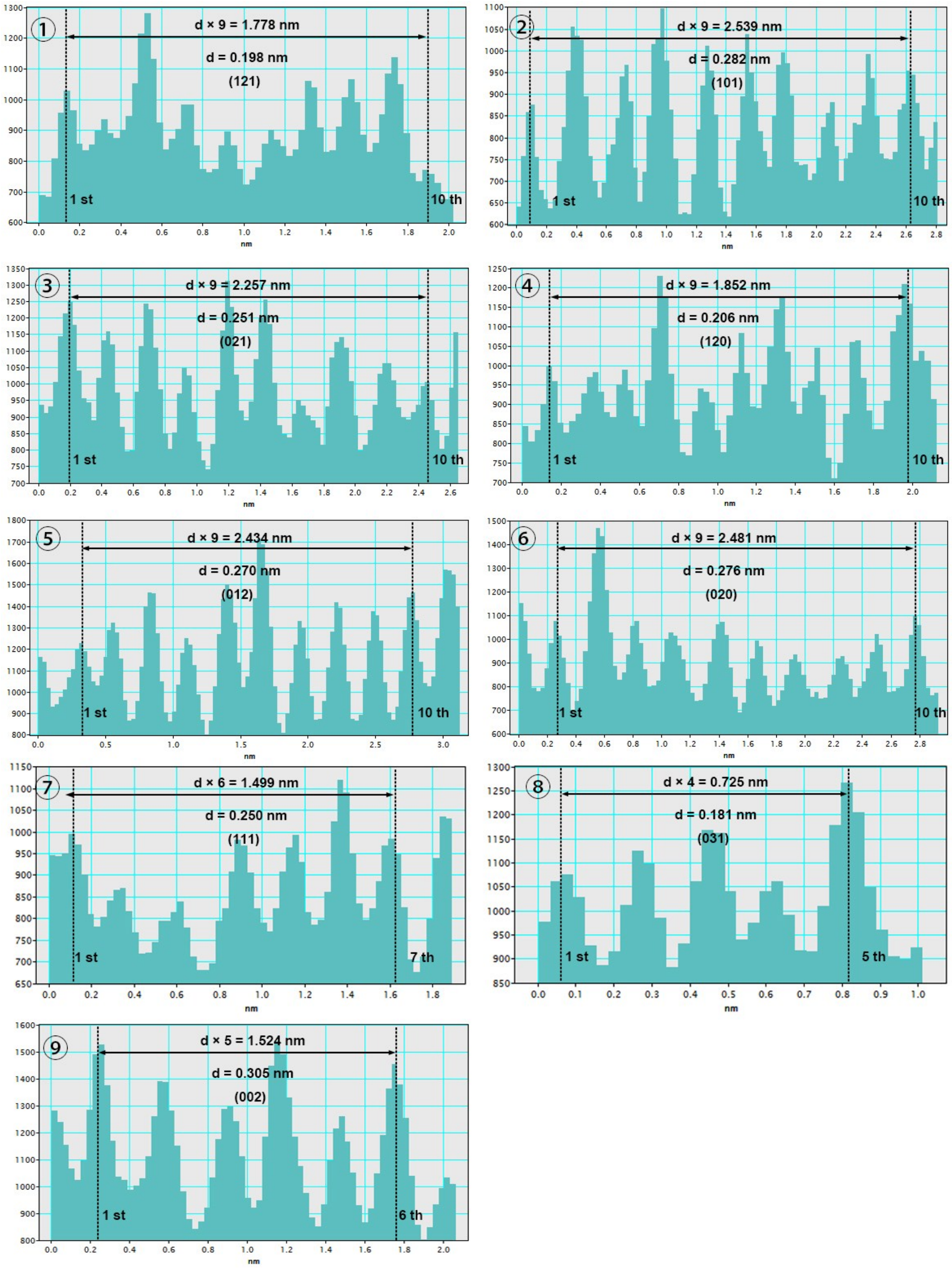

Fig. S13. The typical integral intensity profiles for RuP. The interlayer distances (d) of lattice fringes can be calculated by averaging the distances between adjacent peaks.

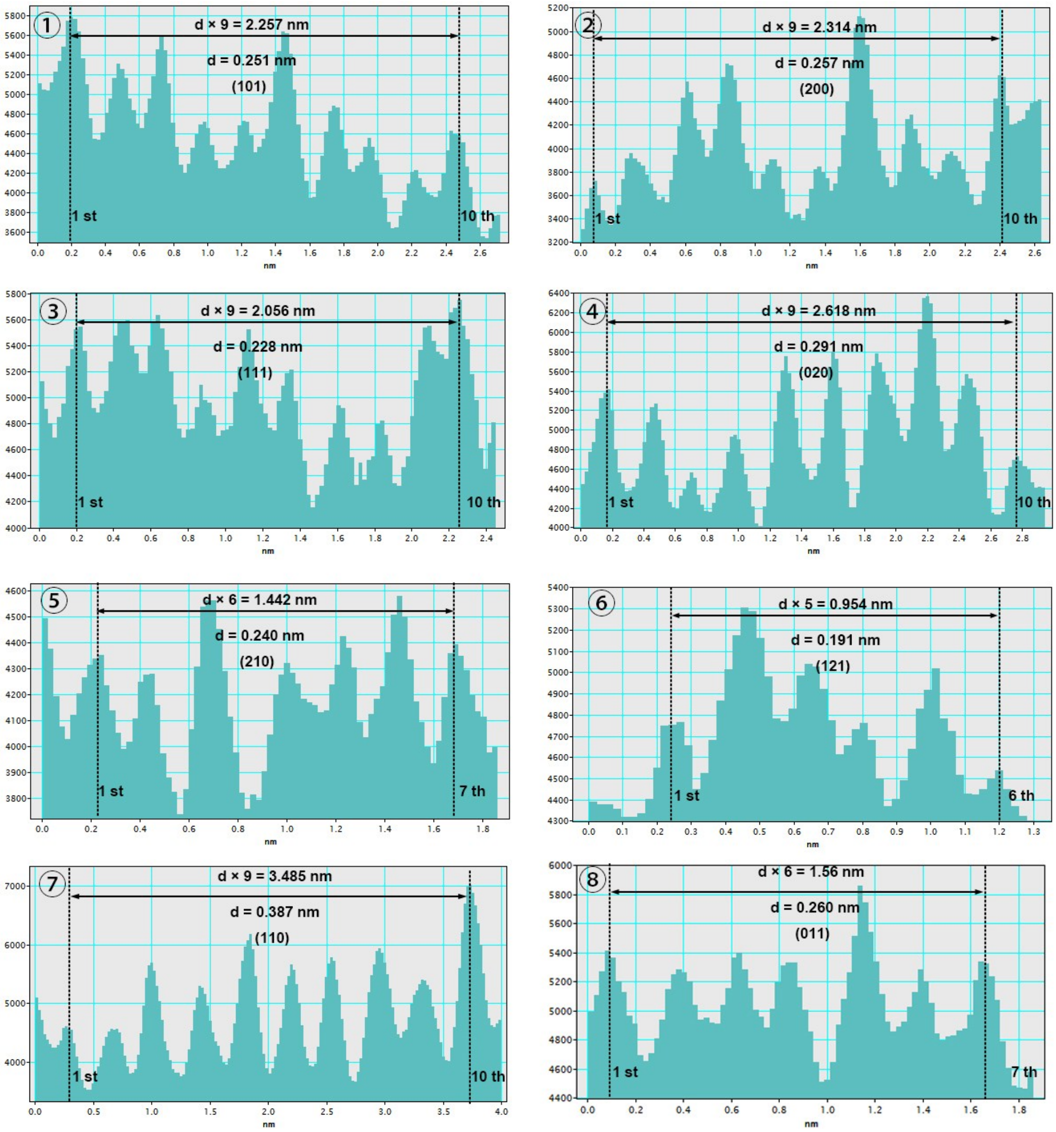

Fig. S14. The typical integral intensity profiles for RuP_2. The interlayer distances (d) of lattice fringes can be calculated by averaging the distances between adjacent peaks .

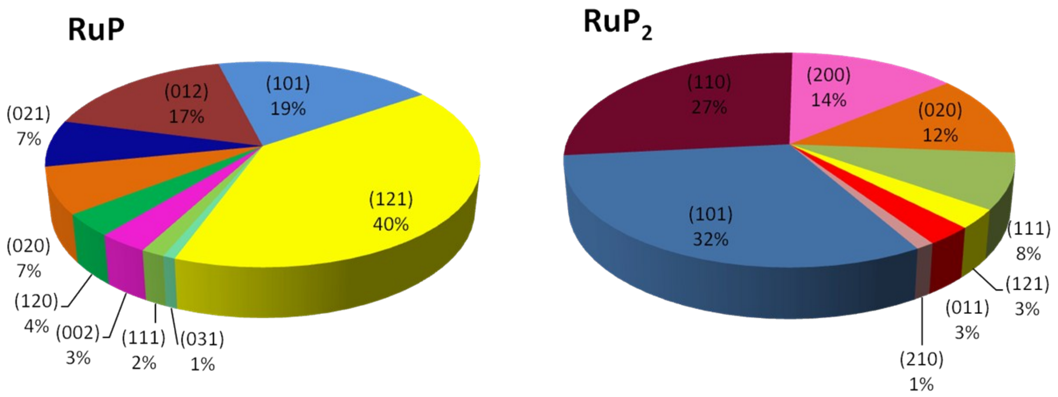

Fig. S15. Distribution diagrams of experimentally observed planes for RuP and RuP$_2$. The intensities were calculated by dividing the area of one facet by the area of all the observed facets. The areas were measured according to the TEM result (Figure S10).

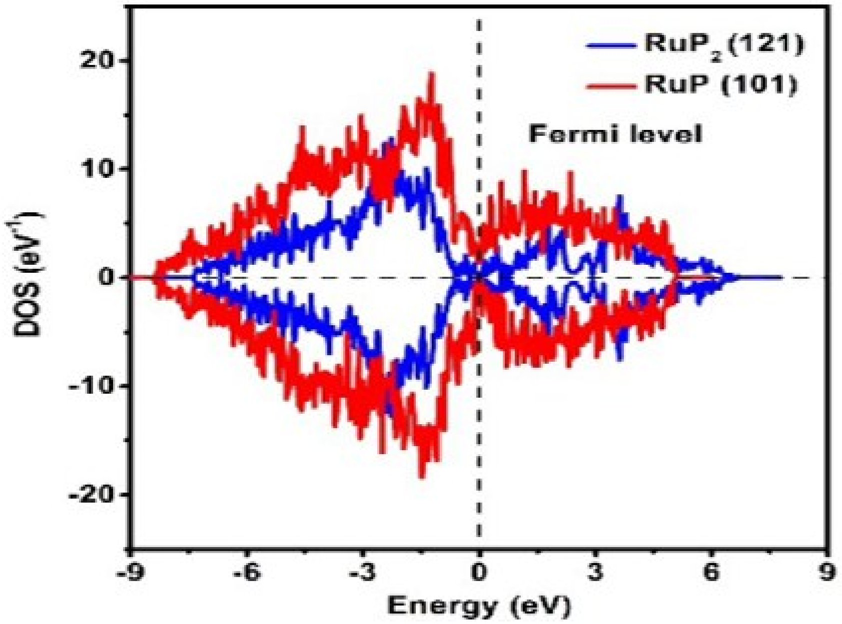

Fig. S16. The DOS of surface Ru atom calculated for RuP (101) surface and RuP$_2$ (121) surface.

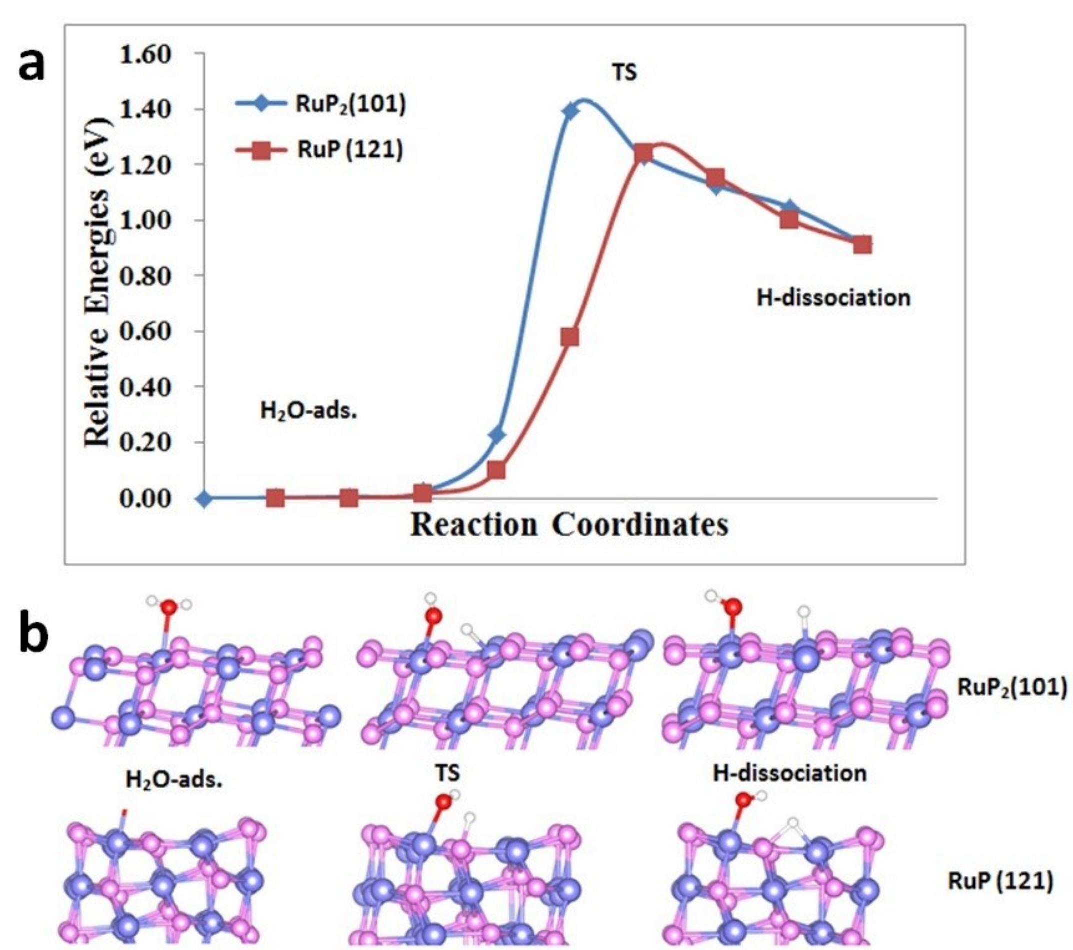

Fig. S17. (a) The calculated water dissociation barrier and (b) water dissociation pathway for RuP (121) and RuP_2 (101) surfaces.

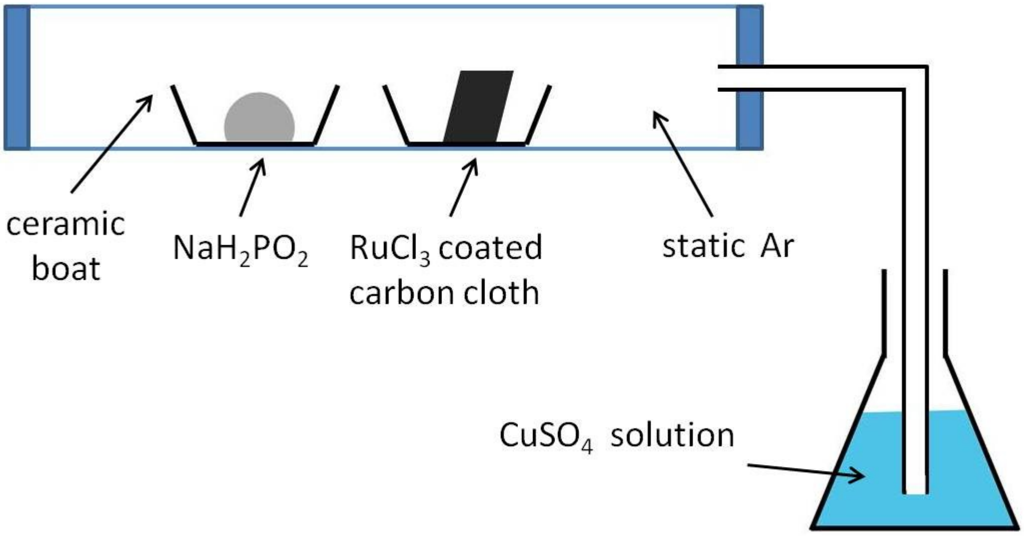

Fig. S18. Illustration of the experimental setup for the preparation of RuP/CC and RuP$_2$/CC. The safety bottle (CuSO$_4$ backflow prevention) is omitted for brevity.

Tab. S1. Comparison of catalytic performance for RuP/CC with other reported electrocatalysts in alkaline media.

Catalyst	substrate	electrolyte	η (mV) at 10 mA cm^{-2}	Ref.
RuP	carbon cloth	1.0 M KOH	13	This work
RuP_2	carbon cloth	1.0 M KOH	33	This work
RuO_2@CN_x	glassy carbon	0.5 M KOH	95	*10*
Ru@N-doped carbon	glassy carbon	0.1 M KOH	28	*11*
Ru–MoO_2	glassy carbon	1.0 M KOH	29	*12*
Pd−Pt	glassy carbon	1.0 M KOH	71	*13*
Ru@C_2N	glassy carbon	1.0 M KOH	17	*14*
RuP_2@N,P dual-doped carbon	glassy carbon	1.0 M KOH	52	*15*
Ru-Co alloy	glassy carbon	1.0 M KOH	28	*16*
Ru-C_3N_4@carbon	glassy carbon	0.1 M KOH	79	*17*
Co@N,B dual-doped carbon	glassy carbon	1.0 M KOH	183	*18*
$Ni(OH)_2/MoS_2$	carbon cloth	1.0 M KOH	80	*19*
Ni_3S_2@porous copper	copper	1.0 M KOH	60.8	*20*
Pt@$Co(OH)_2$	carbon cloth	1.0 M KOH	32	*21*
CoP	titanium foil	1.0 M KOH	60	*22*
$NiCo_2P_x$	carbon cloth	1.0 M KOH	58	*23*
Fe-doped CoP	titanium foil	1.0 M KOH	78	*24*
$Zn_{0.08}Co_{0.92}P$	titanium mesh	1.0 M KOH	67	*25*
TiO_2 decorated Co	carbon cloth	1.0 M KOH	108	*26*
$NiCo_2S_4$	nickel foam	1.0 M KOH	210	*27*
$Ni_{0.89}Co_{0.11}Se2$	nickel foam	1.0 M KOH	85	*28*
Co_3Se_4	nickel foam	1.0 M KOH	45	*29*
c-$CoSe_2$	carbon cloth	1.0 M KOH	190	*30*

$MoNi_4/MoO_{3-x}$	nickel foam	1.0 M KOH	17	*31*
Mo_2C@N-doped carbon	glassy carbon	1.0 M KOH	100	*32*

Tab. S2. Rct values (unit is Ω) of the same RuP/CC sample before and after HER stability test.

Potential (vs. Ag/Ag Cl) Sample	-1.0	-1.03	-1.08	-1.13	-1.18
Before HER	2.920	1.812	0.850	0.620	0.535
After HER	2.139	1.453	0.712	0.611	0.540

Tab. S3. Catalyst loading results of RuP/CC and RuP_2/CC.

Sample	Catalyst loading ($mg\ cm^{-2}$)	Ru loading ($mg\ cm^{-2}$)	P loading ($mg\ cm^{-2}$)
RuP/CC Sample 1	3.3	2.5	0.8
RuP/CC Sample 2	3.1	2.3	0.7
RuP/CC Sample 3	3.5	2.6	0.8
RuP_2/CC Sample 1	3.7	2.3	1.4
RuP_2/CC Sample 2	4.3	2.7	1.6
RuP_2/CC Sample 3	4.2	2.6	1.5

References

[1] G. Kresse, J. Furthmuller, *Comp. Mater. Sci.*, **1996**, *6*, 15–50.

[2] G. Kresse, J. Furthmuller, *Phys. Rev. B*, **1996**, *54*, 11169–11186.

[3] G. Kresse, J. Furthmuller, *Phys. Rev. B*, **1994**, *49*, 14251–14269.

[4] B. Hammer, L.B. Hansen and J.K. Norskov, *Phys. Rev. B*, **1999***,* 59, 7413.

[5] G. Kresse, D. Joubert, *Phys. Rev. B*, **1999**, *59*, 1758–1775.

[6] P. E. Blochl, *Phys. Rev. B*, **1994**, *50*, 17953–17979.

[7] H. J. Monkhorst, J. D. Pack, *Phys. Rev. B*, **1976**, *13*, 5188–5192.

[8] G. Henkelman, B. P. Uberuaga, H. Jónsson, *J. Chem. Phys.*, **2000**, *113*, 9901–9004.

[9] J. K. Nørskov, T. Bligaard, A. Logadottir, J. R. Kitchin, J. G. Chen, S. Pandelov, U. Stimming, *J. Electrochem. Soc.*, **2005**, *152*, J23–J26.

[10] T. Bhowmik, M. K. Kundu, S. Barman, *ACS Appl. Mater. Interfaces* **2016**, *8*, 28678–28688.

[11] X. Chen, J. Zheng, X. Zhong, Y. Jin, G. Zhuang, X. Li, S. Deng, J.-G. Wang, *Catal. Sci. Technol.* **2017**, *7*, 4964–4970.

[12] P. Jiang, Y. Yang, R. Shi, G. Xia, J. Chen, J. Su, Q. Chen, *J. Mater. Chem. A* **2017**, *5*, 5475–5485.

[13] J. Fan, K. Qi, L. Zhang, H. Zhang, S. Yu, X. Cui, *ACS Appl. Mater. Interfaces 2017*, ***9***, 18008–18014.

[14] J. Mahmood, F. Li, S. M. Jung, M. S. Okyay, I. Ahmad, S. J. Kim, N. Park, H. Y. Jeong, J. B. Baek, *Nat. Nanotechnol.* **2017**, *12*, 441–446.

[15] Z. Pu, I. S. Amiinu, Z. Kou, W. Li, S. Mu, *Angew. Chem., Int. Ed.* **2017**, *56*, 11559–11564.

[16] J. Su, Y. Yang, G. Xia, J. Chen, P. Jiang, Q. Chen, *Nat. Commun.* **2017**, *8*, 14969.

[17] Y. Zheng, Y. Jiao, Y. Zhu, L. H. Li, Y. Han, Y. Chen, M. Jaroniec, S. Z. Qiao, *J. Am. Chem. Soc.* **2016**, *138*, 16174–16181.

[18] H. Zhang, Z. Ma, J. Duan, H. Liu, G. Liu, T. Wang, K. Chang, M. Li, L. Shi, X. Meng, K. Wu, J. Ye, *ACS nano* **2016**, *10*, 684–694.

[19] B. Zhang, J. Liu, J. Wang, Y. Ruan, X. Ji, K. Xu, C. Chen, H. Wan, L. Miao, J. Jiang, *Nano Energy* **2017**, *37*, 74–80.

[20] C. Yang, M. Gao, Q. Zhang, J. Zeng, X. Li, A. P. Abbott, *Nano Energy* **2017**, *36*, 85–94.

[21] Z. Xing, C. Han, D. Wang, Q. Li, X. Yang, *ACS Catal.* **2017**, *7*, 7131–7135.

[22] D. Zhou, L. He, W. Zhu, X. Hou, K. Wang, G. Du, C. Zheng, X. Sun, A. M. Asiri, *J. Mater. Chem. A* **2016**, *4*, 10114–10117.

[23] R. Zhang, X. Wang, S. Yu, T. Wen, X. Zhu, F. Yang, X. Sun, X. Wang, W. Hu, *Adv. Mater.* **2017**, *29*, 1605502.

[24] C. Tang, R. Zhang, W. Lu, L. He, X. Jiang, A. M. Asiri, X. Sun, *Adv. Mater.* **2017**, *29*, 1602441.

[25] T. Liu, D. Liu, F. Qu, D. Wang, L. Zhang, R. Ge, S. Hao, Y. Ma, G. Du, A. M. Asiri, L. Chen, X. Sun, *Adv. Energy Mater.* **2017**, *7*, 1700020.

[26] J. X. Feng, H. Xu, Y. Dong, X. Lu, Y. Tong, G. Li, *Angew. Chem., Int. Ed.* **2017**, *129*, 3006–3010.

[27] A. Sivanantham, P. Ganesan, S. Shanmugam, *Adv. Funct. Mater.* **2016**, *26*, 4661.

[28] B. Liu, Y. Zhao, H. Peng, Z. Zhang, C. K. Sit, M. F. Yuen, T. Zhang, C. Lee, W. Zhang, *Adv. Mater.* **2017**, *29*, 1606521.

[29] W. Li, X. Gao, D. Xiong, F. Wei, W.-G. Song, J. Xu, L. Liu, *Adv. Energy Mater.* **2017**, *7*, 1602579.

[30] P. Chen, K. Xu, S. Tao, T. Zhou, Y. Tong, H. Ding, L. Zhang, W. Chu, C. Wu, Y. Xie, *Adv. Mater.* **2016**, *28*, 7527.

[31] Y. Chen, Y. Zhang, X. Zhang, T. Tang, H. Luo, S. Niu, Z. Dai, L. Wan, J. Hu, *Adv. Mater.* **2017**, *29*, 1703311.

[32] Y. Huang, Q. Gong, X. Song, K. Feng, K. Nie, F. Zhao, Y. Wang, M. Zeng, J. Zhong, Y. Li, *ACS nano* **2016**, *10*, 11337–11343.